Time-dependent reliability analysis of overpacks for high-level radioactive waste

A. Persoons, P. Beaurepaire, A. Chateauneuf, F. Bumbieler

Time-dependent reliability analysis of overpacks for high-level radioactive waste

A. Persoons, P. Beaurepaire, A. Chateauneuf
Université Clermont Auvergne, CNRS, SIGMA Clermont, Institut Pascal, F-63000 Clermont-Ferrand, France

F. Bumbieler
Andra, 1 Rue Jean Monnet, 92290 Châtenay-Malabry, France

Abstract: In France, nuclear energy is extensively used for electricity production, and consequently high-level radioactive waste are generated by the fleet of nuclear powerplants. This waste is planned to be disposed of in a deep geological repository. Engineers have only a limited feedback from similar disposal facilities, as this project is innovative. This lack of knowledge and the timescales involved induce uncertainties about the disposal environment and about the conditions of operation. Reliability analysis is used here as it provides a suitable framework to deal with such uncertainties. This paper focuses on the overpack, which isolates the waste from the environment during the early stage of disposal (at least 500 years). The failure probability is investigated through a crack propagation criterion using a Monte Carlo analysis performed on two levels. The approach is based on a dedicated stochastic structural model including the corrosion rate, the mechanical loading and initial crack conditions. The robustness of this approach is evaluated through sensitivity analysis, and by considering multiple distributions for the variables elicited from expert's opinion.

1. Introduction

About 10.6% of world electricity production (International Energy Agency 2017) and 70% of the French electricity production in 2015 is generated by nuclear power plants. The management of the radioactive waste resulting from this industry is an important issue. The European council directive 2011/70/EURATOM states that, at this time, deep geological repository is the safest option as the end point of management of high-level radioactive waste. The methodology has been studied for several decades, including laboratory tests, as well as the construction and operation of in-situ underground research facilities, and is currently considered as the most feasible way of management of radioactive waste (Chijimatsu et al. 2005; W. R.Alexander and Linda McKinley 2007; Rempe 2007; Lidskog and Andersson 2002; Levy 2010). Deep geological repositories are investigated as an option for radioactive waste management in many countries including Belgium, Canada, Czech Republic, Finland, France, Germany, Hungary, Japan, Sweden, Switzerland and the USA (International Atomic Energy Agency 2001; Lidskog and Andersson 2002). However, since the waste and the nature of the ground of every site are different, minimizing the risk of pollution requires facilities specifically engineered for each project. The work presented in this paper falls within the framework of Cigéo which is the French project of deep geological repository for Intermediate Level Long-Lived and High Level radioactive waste.

In this project high-level radioactive waste (HLW) is planned to be conditioned in non-alloy steel overpacks and inserted in horizontal micro-tunnels. The main role of the overpack is to isolate the waste from the environment long enough to significantly decrease its radiotoxicity and heat, which is estimated to 500 years. Every overpack is inspected for manufacturing defects such as cracks, inclusions or cavities. However, in operating conditions the overpack may display manufacturing defects smaller than the detection threshold, in addition to be subjected to corrosion and mechanical loading. Moreover, as

for every engineered system, this overpack is subjected to design and environmental uncertainties. These uncertainties are related to the extrapolation of phenomena over long time periods and limited amount of available data induced by the novelty of the project, making the analysis challenging. The uncertainties about the operating conditions induce uncertainties about the integrity of the system along the disposal time justifying the use of reliability methods (Hari Prasad et al. 2013; Kim et al. 2013; Bhargava, Mori, and Ghosh 2011).

The reliability methods have not been explored yet for the HLW facilities but they are already vastly used for facilities with comparable constraints such as underground pipelines (Dundulis et al. 2016; Amirat, Mohamed-Chateauneuf, and Chaoui 2006). These methods are based on the stochastic structural approach, in which a mechanical model of the system is associated with uncertainties and used in a reliability-based calculation procedure. It allows the estimation of the probability of occurrence of a failure event (the failure probability) related to the response of the model (Lemaire 2013; Schuëller 1989). In this study the reliability method is coupled with a dedicated finite element model. Moreover, as the failure event is rare, the numerical evaluation of the failure probability may involve a large number of simulations. Hence, the issues in designing such a model are the computational time and the parameterization to implement the variabilities (Sudret and Der Kiureghian 2002; Stefanou 2009; Patelli et al. 2012). The reliability methods aim at reducing the number of numerical evaluations necessary to estimate the probability of failure and increasing the accuracy of this estimation.

The failure event studied is the propagation of a pre-existing crack, it is associated with a fracture mechanics criterion. For the sake of this analysis, a finite element (FE) model of the overpack including the corrosion process is developed, allowing to consider the uncertain corrosion rates and mechanical loadings. The time dependence is handled by carrying out independent static FE calculations at several time steps until failure. A post-processing procedure is developed as well, allowing to simulate surface cracks with uncertain positions and orientations from the results of the FE model. These features allow us to analyse a large number of crack configurations with moderate numerical efforts. The reliability is studied using a Monte-Carlo procedure based on two levels to maximise the number of simulations. The sensitivity of the stress intensity factor is studied with respect to the input parameters as well as the sensitivity of the failure probability with respect to the type of probability distribution. The interest of this work is the deployment of structural reliability methods to a component of radioactive waste repository problems.

The procedure of the analysis follows 3 steps: first a realisation of the random variables is generated; second, the finite element (FE) model is evaluated for several time steps until complete corrosion of the overpack; third, for each time step, the stress intensity factors associated with various randomly generated cracks are evaluated and compared to the critical stress intensity factor K_{1scc} to detect the failure.

The upcoming section of the paper presents an overview of the studied system and the main issues of the analysis. Then the stochastic structural model developed for the study is presented in details as well as the design features and the applied reliability method. The results of Monte-Carlo simulations and of sensitivity analyses are presented and discussed in section 3. The paper closes with the conclusions and outlook.

2. Overpack operating conditions

Deep geological repositories are designed as the end point of management of radioactive wastes of high and long-lived intermediate level activity. The disposal facilities are considered as multi-barrier systems where geological and engineered barriers work together as Russian nesting dolls to contain and isolate the waste from the biosphere. The design of the Cigéo project is based on an impermeable geological clay rock formation (Callovo-Oxfordian claystone) able to contain the radioactivity over a long period

of time (ANDRA 2005). Underground facilities (access drifts, disposal cells) will be drilled in the middle of the layer at 500m depth, one of them is shown in fig. **1.a.** Such galleries are dedicated to handling operations. HLW diposal cells are horizontal micro-tunnels of about 0.9 m in diameter. A non-alloy steel liner is inserted in the micro-tunnel, and a cement-based filling material is injected between the liner and the rock for corrosion issues. HLW waste packages will be inserted inside the cell. They consist of non-alloy steel overpacks, containing a stainless-steel primary package, inside of which the vitrified waste is cast (fig. **1.b**). A premature contact between the water and the primary package may lead to an accelerated degradation of the glass matrix of the radioactive waste (Hoorelbeke 2009). Therefore, the function of the overpack is to isolate the package from the environment long enough to sufficiently decrease its radiotoxicity and heat. Moreover, one of the major goals of the Cigéo project is the reversibility period. The principle is that for the first 100 years of operation, every waste package can be extracted at any time for limited cost. This requirement implies a mechanical stability of the steel liner to allow the access to the waste for the first 100 years.

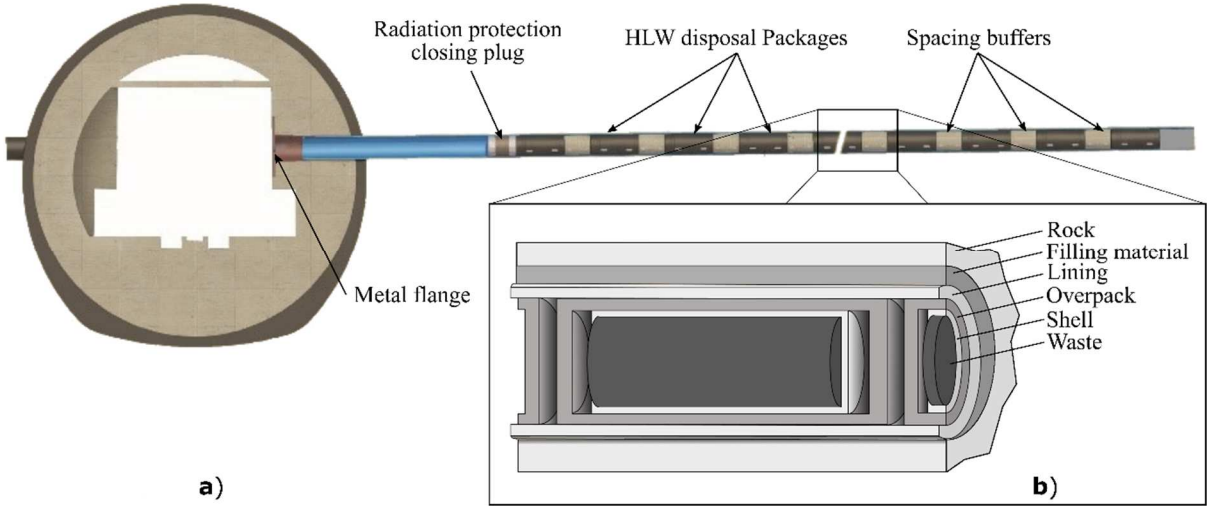

Figure **1.** Overview of the HLW facilities as planned for the Cigéo project. **a.** General aspect of the HLW cell (courtesy of Andra). **b.** Russian nesting doll like barrier system

The first issue affecting the overpack in repository conditions is the corrosion. The argillaceous rock contains water that may flow into the cells, this process is expected to progressively fill the HLW cell and is represented by a time-dependant water level in the cell. The evolution of the water level is defined by the following scenario. During the reversibility phase, a liquid water extraction system keeps the tunnel dry. After this period the evolution of the water level results from the equilibrium of liquid and gas phases in the cell, it has been studied by Croisé et al. (2011) for long-lived intermediate level waste disposal cells in the project, i.e. considering the same rock layer. The results state that the rock saturation increases and the water flows in. After a while, an equilibrium is reached between the water and gas pressure and the water level stabilises to a constant value. This study focuses only on the case of a water level stabilizing at an intermediate value filling half of the cell. The water induces two different corrosion rates in the cell, one in water and one in wet atmosphere. The values and evolutions of these corrosion rates are the results of chemical processes which are uncertain. The proposed evolution relies on in-situ studies lead on the corrosion process of the overpack (Schlegel et al. 2014; Necib et al. 2017) and the details about these uncertainties are given in section 3.2. Therefore, at each point of the overpack, the corrosion rate is environment-dependent and the environment is time-dependent (related to the evolution of the water level). Moreover, the corrosion rates in both environments are time-dependent and uncertain. These processes induce a non-uniform corrosion of the overpack leading to a complex and uncertain geometry of the corroded profile.

The second issue the overpack faces in operating conditions is related to mechanical loading. After the reversibility phase, the cells are closed and the access drifts backfilled so that the atmosphere in the cell

will progressively reach a pressure equilibrium with the surrounding rock, resulting in the overpack being subjected to a uniform fluid pressure. Then, the corrosion process affecting the liner will progressively reduce its effective thickness. This thickness reduction coupled with the rock pressure will cause the buckling of the liner, which will come into contact with the overpack and transmit the rock pressure. The buckling time is estimated by an empirical law established in earlier studies by Ngyuen (2017). This model considers the buckling of an infinite confined cylinder subjected to an external pressure. The contact area progressively grows as the corrosion reduces the thickness of the liner and additional buckling occur. At long term (i.e. long after the total corrosion of the liner) contact area tends to completely surround the overpack, the rock pressure is then directly applied to the overpack; this loading is also uncertain. As a result, the mechanical loading is composed of a constant and deterministic fluid pressure, and a time dependant (related to the evolution of the contact area) and uncertain contact pressure.

The last issue taken into account in the model is a potential manufacturing flaw in the material. The overpack is a welded assembly of 3 forged parts in low carbon steel (fig. **2**). This material is chosen because it has been widely used during the past decades (in civil engineering, in the pressure vessel industry, etc.), it is easily weldable, its corrosion process is more predictable than stainless steel, in addition to its good ductility properties. The top welding is more difficult to carry out because the package is already in the overpack. There are also constraints limiting the heat treatment necessary to reduce the residual stress in the welding. Each overpack is inspected to detect possible flaws in the material. It is then assumed that no flaw bigger than the detection threshold can remain undetected. However smaller flaws are likely to remain in the in-situ overpacks, and their position and orientation are uncertain. These flaws may have a critical effect on the overpack failure. In this study, surface flaws are modelled by randomly generated semi-elliptical surface cracks that may initiate a fracture.

Figure **2**. R7-T7 vitrified waste disposal package

The failure mode investigated in this paper is the fracture of the overpack due to the propagation of an initial crack. The fracture occurs when the stress intensity factor exceeds a threshold value as described by the linear elastic fracture mechanics. Even if general corrosion is the main corrosion mode expected for the overpack, brittle fracture has been studied to cover, in a safe design approach, the case of a potential Stress Corrosion Cracking (SCC) or hydrogen embrittlement sensitivity of the steel in repository conditions. Therefore, the failure criterion involves the SCC fracture toughness of the material K_{1scc}, whose value is uncertain. The distribution affected to K_{1scc} is discussed in section 3.2. It relies on a study of the fracture toughness of the overpack under stress corrosion cracking conditions (Necib et al. 2017), in which CT specimens have been loaded to 40 MPa$\sqrt{m}$ during 4000 hours

exhibiting very limited propagation (<150 µm).

3. Methods of analysis

This section discusses the applied strategy to implement the stochastic structural model of the overpack. This implementation requires to identify the boundary conditions properly describing the in-situ conditions, to build a dedicated FE model designed to be adaptable and robust enough to take into account the uncertainties and the evolution of the geometry over time. The reliability analysis method considered is a two levels Monte Carlo method based on the stochastic and time-dependent FE model.

3.1. Evolution of the mechanical loading

As indicated in section 2, the mechanical loading is composed of a constant fluid pressure and a time-dependent and uncertain soil-liner pressure. The fluid pressure is defined in the FE model as a uniform external pressure with the constant value of 5MPa corresponding to the in-situ pore pressure in the rock. Defining the contact loading applied at the outer face of the overpack requires first to identify the evolution of the contact area between the overpack and the buckled liner over time. The contact area is composed of two diametrically opposed areas defined by a contact angle α and representing the expected buckling mode (fig. **3.a**). The circumferential orientation of the contact areas is highly unpredictable because it depends on local material and loading heterogeneities. Horizontal orientation has been considered, to take into account the anisotropy of the excavation induced fracture network (Bumbieler et al. 2015) which may result in a lower stiffness of the surrounding rock in this direction. As long as the buckling of the liner has not occurred, the contact angle is equal to zero, and no corresponding load is applied. The estimation of the buckling time using the law introduced in section 2 considers the rock pressure, the initial thickness and the corrosion rate. The post-buckling behaviour and the expansion of the contact areas, driven by the rock mechanical properties, is difficult to predict. It is then assumed, as a first approximation, that α increases linearly such that it reaches 180° after 3000 years. The pressure profile on the contact area is parabolic such that the pressure is equal to zero at the edges of the contact area and to its nominal value (P_c) in the middle (fig. **3.b**). Hence, the expression of the contact applied pressure is given by: $P(\theta,t) = P_c.h(\theta,t)$ with.

$$h(\theta,t) = \begin{cases} \text{if } \alpha(t) < 180, \theta \in \left[\frac{-\alpha}{2}, \frac{\alpha}{2}\right], h(\theta,t) = 1 - \left(\frac{2\theta}{\alpha(t)}\right)^2 \\ \text{if } \alpha(t) \geq 180, \theta \in [-90, 90], h(\theta,t) = 1 - \left(\frac{2\theta}{\alpha(t)}\right)^2 \end{cases}$$

where P_c defines the amplitude of the applied pressure and carries all the uncertainties, h(θ,t) is a function of maximal value equal to 1, and carries the variation of pressure in time and space. The distribution of P_c is detailed in section 3.2. For α greater than 180°, the evolution of the pressure profile is adapted so it tends to a circular profile, representing the overpack directly subjected to an isotropic rock pressure. It represents the isotropic in-situ stress field in the cross-section of disposal cells which are planned to

be drilled parallel to major principal stress σ_H (Bumbieler et al. 2015).

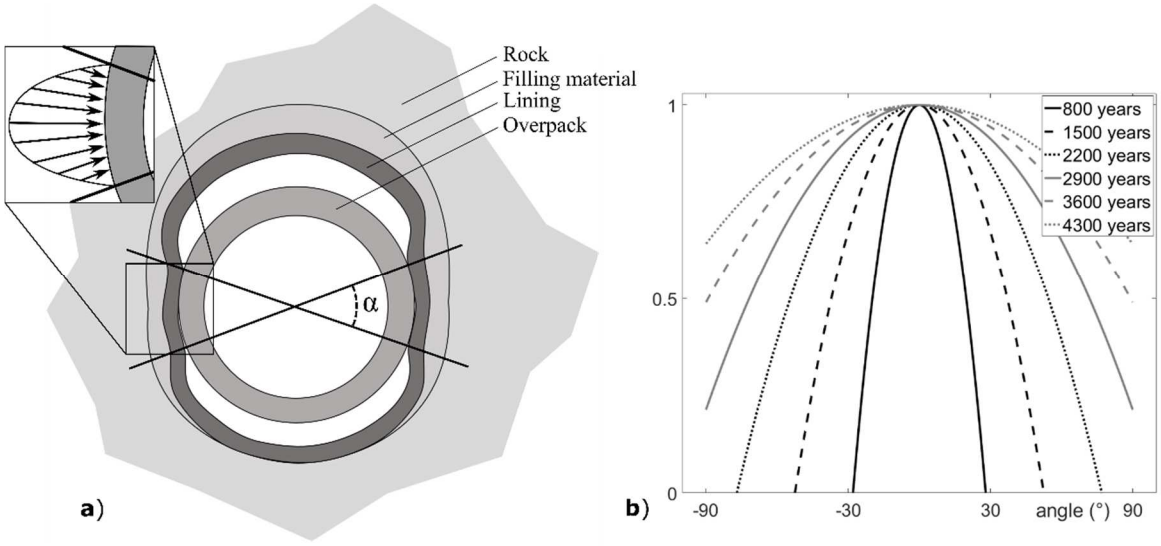

Figure **3.a.** Schematic drawing of the contact angle **b.** Pressure profile for several time steps after buckling

3.2. Modeling of the uncertainties

As introduced in section 2, the water level is time-dependent according to the evolution presented in figure **4.b.** It induces two corrosion rates, CR_a and CR_w in the wet atmosphere and under water, respectively. During the reversibility phase a possible inflow of oxygen from the access gallery is taken into account and the corrosion rates are therefore considered steady for the first 100 years. After this period, the corrosion rates decrease until reaching a new equilibrium state (fig. **4.a**). The uncertainties related to both corrosion rates may be associated with uncertainties about the kinetics of the chemical processes due to uncertainties about environmental conditions evolution. Moreover, the involved material and the environment are the same for both corrosion rates. As a result, if the corrosion rate in the water is higher than the value predicted by the expert, the corrosion rate in the atmosphere is very likely to be higher than the expert prediction as well. Therefore, the corrosion rates and their values over time are considered as fully correlated and are affected by only one random variable C defined as a

multiplying factor applied to the evolution curves of both corrosion rates.

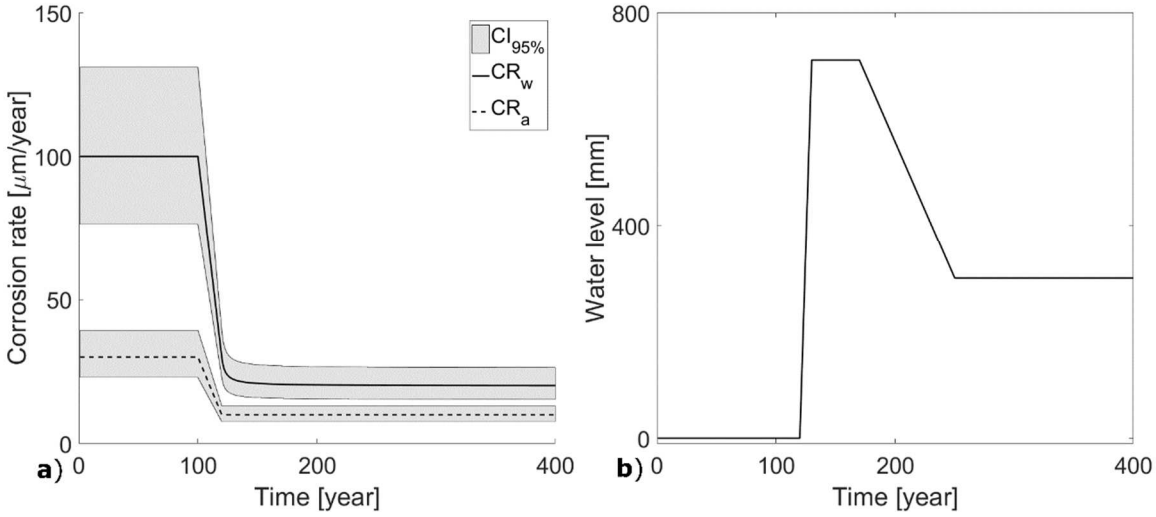

Figure **4.a.** Evolution curve of the corrosion rates and the 95% confidence intervals associated to their probability density function **b.** Evolution curve of the water level

The distribution of C has been elicited from expert's judgment. The expert believes that the corrosion rates have a nominal value c and that the credible interval that is the most likely to contain the actual value is $\left[\frac{1}{1.5}c\ ;\ 1.5c\right]$. The lognormal distribution is chosen because a random variable following such a distribution is equally likely to be greater than k and smaller than $\frac{1}{k}$ which fits the expert's confidence interval. By considering that the amplitude of the confidence interval equal to 6 times the standard deviation, 99.7% of the realisations of C fall in the expert's interval.

The contact pressure resulting from the transmission of the rock pressure to the overpack after buckling is uncertain. The experts estimate the pressure to be most likely in the interval $\left[\frac{1}{2}P_c\ ;\ 2P_c\right]$ with P_c = 8MPa. The same strategy applied for corrosion is again used to define a log-normal distribution for the contact pressure.

The position and orientation of cracks in the overpack are characterized by two angles θ_p and θ_o respectively (figs. **5.a, 5.b**).Where θ_p is the angle characterizing the position of the crack with respect to the horizontal axis of the cross-section of the FE model and θ_o is the angle between the major axis of the crack and the circumferential axis of the FE model, it characterizes the orientation of the crack on the surface of the overpack. As a first approximation, it is assumed that the crack does not exhibit preferential position nor orientation. Therefore, uniform densities of range 180° are assigned to both θ_p and θ_o.

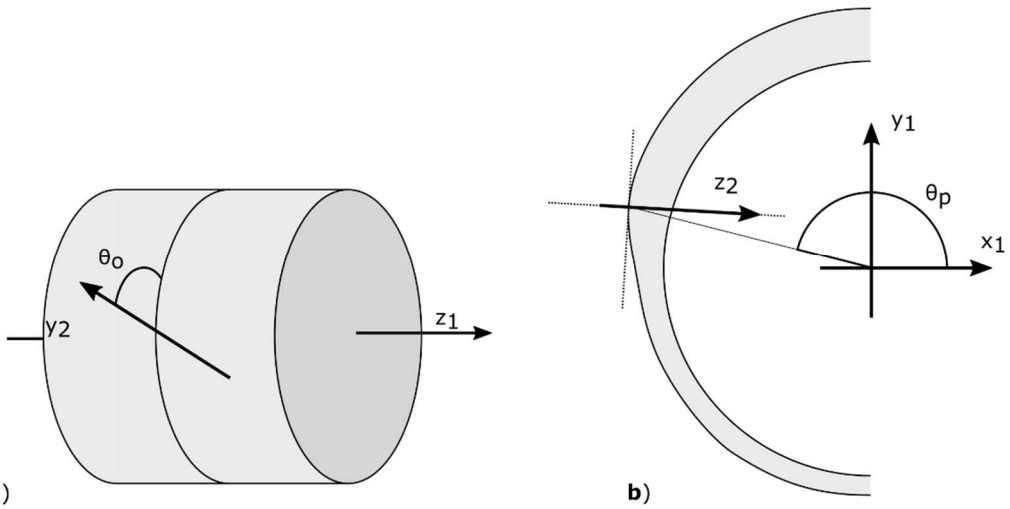

Figure **5.a.** Crack orientation angle, **b.** Crack position angle

As discussed in section 2 the fracture toughness of the overpack has been investigated in a study and further studies are in progress but no statistical data are currently available. This lack of data prevents us from identifying the distribution type and it is reasonably decided to model the fracture toughness with a normal distribution with mean value of 40 MPa$\sqrt{\text{m}}$ and coefficient of variation of 0.1

3.3. Evolution of the corroded profile

The corrosion leads to a reduction of the overpack wall thickness. As a result, the cross-section of the overpack is expressed in terms of time and corrosion rates, and its calculation requires a proper definition of the corrosion rates and water level functions (see section 3.2).

The corroded thickness can be calculated at every time step and for every point of the cross-section, by considering the water level and corrosion rate functions. In order to define the corroded geometry, the corroded thickness is calculated at 16 points of the cross-section, and the geometry is defined by the spline curve passing through these points (fig. **6**). The spline curve is then used to define the cross-section of the FE model. As a first approximation the model is limited to the elastic behaviour of the material to reduce the computational time. The FE model is composed of a tetrahedral quadratic mesh to ensure that the mesh can be automatically generated for all the possible geometries of the corroded overpack. The FE model is evaluated for time steps of 100 years until complete corrosion of the overpack. The model is linear elastic, therefore it does not dependent on the loading history and independent static simulations are carried out at each time step. The time step is chosen as to ensure

good precision with reasonable computation time.

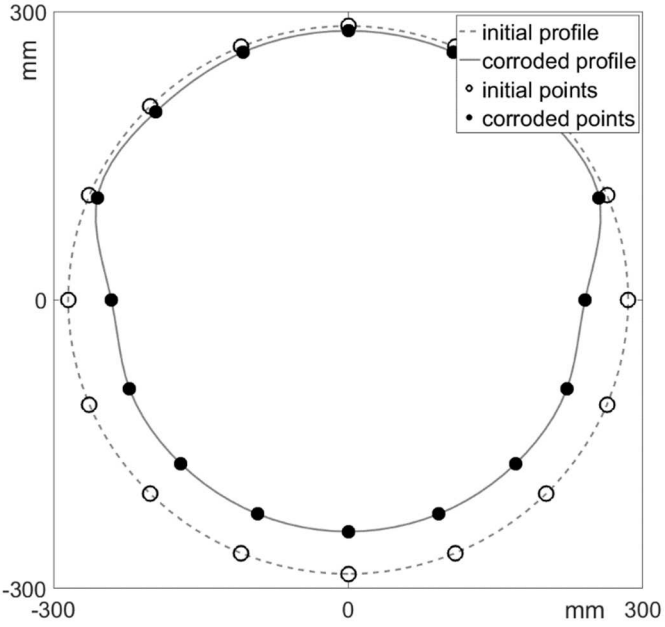

Figure **6** Geometry of the modelled cross-section of the corroded overpack

3.4. Simulation of the crack

The failure mode investigated in this study is the propagation of a pre-existing crack. It is assumed that the flaws introduced by the manufacturing process can be modelled as semi-elliptical cracks. The dimensions of the crack are taken as the biggest acceptable flaw, according to quality control described in the European standards (AFNOR 1998) regarding non-destructive testing of forged parts. Therefore, the geometry of the crack is deterministic with both depth d_c and length l_c of 2mm (fig. **8**); this value is considered as upper bound for both dimensions. In order to reduce the computational time, the crack is not directly modelled in the FE mesh, instead the crack is simulated by post-processing the results of the uncracked model. As the reliability analyses implying a complex third-party model are generally limited by the computational time (Patelli et al. 2012; Broggi and Schuëller 2011; Valdebenito and Schuëller 2010; Goller et al. 2011), this strategy allows us to simulate numerous crack configurations from a single evaluation of the FE model.

The stress intensity factor of the opening mode (K_1) is evaluated by Pommier et al. (1999) as a generalization of the work of Newman and Raju (1981). The strategy used consists of modelling the strain of un-cracked material and recovering the stress at the crack location. The stress intensity factor is then deduced from the stress field. This approach is valid when the size of the crack is small compared to the dimensions of the un-cracked ligament. The inputs of this model are the crack dimensions and a space-dependent polynomial expression of the stress field associated with the opening mode of the crack. The stress must be expressed in the coordinate system associated with the crack, and only the stress orthogonal to the crack plan is necessary. The method is applicable only for semi-elliptical s cracks and gives good estimations of K_1 for a wide range of crack sizes and stress fields.

Hence, a polynomial expression of the stress field of the un-cracked model around the crack position is required for the calculation of the stress intensity factor. The procedure consists of recovering the stress tensor at several geometrical locations around the crack position. Then a polynomial expression of each component of the tensor is fitted by least square regression. The most direct approach would be to

retrieve the data at several locations around the crack for each simulated crack, however the data retrieving process can be time-consuming. Hence the data are instead recovered only once but at locations distributed in all the area where the crack can be simulated. Only one data extraction is then necessary to simulate all possible crack positions. Moreover, to reduce the data extraction time, the possible crack locations are limited to the external surface of the overpack at one longitudinal position (z_c). The conservatism of the model is ensured by choosing z_c to match the highest tensile stress concentration area. Therefore the stress tensor is retrieved at all points of a 3D grid centred on z_c and composed of 700 circumferential points, five longitudinal points and five radial points. The grid width and depth are $3l_c$ and $3d_c$ respectively (fig. 7). The detailed procedure of the regression and the rotation in the local coordinate system associated with the crack, is as following:

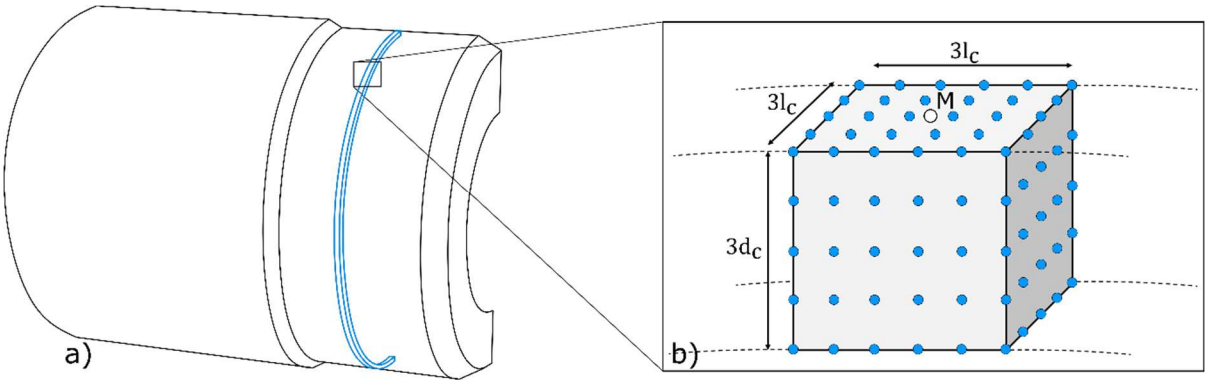

Figure **7.a.** Schematic representation of the grid of data recovering points **b.** Schematic representation of the slice of gird centred on the crack position used for the regression

Let B_1 denotes the coordinate system associated with the overpack (i.e. the global coordinate system defined in the FE model) and B_2 denotes the local coordinate system associated with the crack (defined by the orientation of the major and minor axes of the crack) as presented in fig. **8**, the transfer matrix expressing the change of coordinate system from B_1 to B_2 is expressed as:

$$M_{B_1}^{B_2} = \begin{pmatrix} -sin(\theta_n)\,sin(\theta_o) & sin(\theta_n)\,cos(\theta_o) & -cos(\theta_n) \\ cos(\theta_n)\,sin(\theta_o) & -cos(\theta_n)\,cos(\theta_o) & -sin(\theta_n) \\ -cos(\theta_o) & -sin(\theta_o) & 1 \end{pmatrix} \quad (1)$$

Let also θ_n denote the angle between $\overrightarrow{z_2}$ the major axis of the crack (fig. **8**) and the horizontal axis of the global coordinate system $\overrightarrow{x_1}$ in the plan shown in (fig. **5.b**). The stress tensors expressed in both coordinate systems are denoted by $\sum^{B_1}$ and $\sum^{B_2}$ such that the term in the first row and the first column of $\sum^{B_1}$ is the tensile stress in the x-direction of the coordinate system B_1. The transfer relationship is expressed as:

$$\left[\sum^{B_2}\right] = \left[M_{B_1}^{B_2}\right]\left[\sum^{B_1}\right]\left[M_{B_1}^{B_2}\right]^t \quad (2)$$

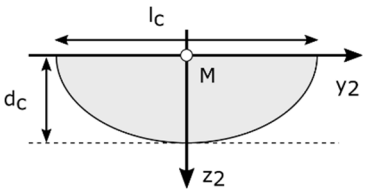

Figure **8.** Geometry of the crack and associated coordinate system

For each realisation of the crack position (symbolized by the point M), a polynomial regression of the stress tensor is performed based on the stress data in the grid centred at the crack location, as shown in

fig.*7***.b**. The polynomial expression is:

$$\left[\sum^{B_1}\right] = [A] + [B]x_1 + [C]y_1 + [D]z_1 \quad (3)$$

where x_1, y_1 and z_1 denote respectively the x, y and z coordinates in the coordinate system of the overpack B_1. The four matrices A, B, C, and D are identified for each component of the stress tensor by least square regression. Combining equations 2 and 3 results in the following expression:

$$\left[\sum^{B_2}\right] = \left[M_{B_1}^{B_2}\right][A]\left[M_{B_1}^{B_2}\right]^t + \left[M_{B_1}^{B_2}\right][B]\left[M_{B_1}^{B_2}\right]^t x_1 + \left[M_{B_1}^{B_2}\right][C]\left[M_{B_1}^{B_2}\right]^t y_1 + \left[M_{B_1}^{B_2}\right][D]\left[M_{B_1}^{B_2}\right]^t z_1 \quad (4)$$

This expression gives the stress field in the crack coordinate system. The transfer from the coordinate system B_2 to the coordinated system B_1 is defined as following:

$$\begin{pmatrix} x_1 \\ y_1 \\ z_1 \end{pmatrix} = \begin{bmatrix} x_c \\ y_c \\ z_c \end{bmatrix} + \left[M_{B_1}^{B_2}\right] \begin{bmatrix} x_2 \\ y_2 \\ z_2 \end{bmatrix} \quad (5)$$

where x_c, y_c, z_c and x_2, y_2, z_2 denote respectively the coordinates of the crack position expressed in the coordinate system of the overpack B_1 and the coordinates in the local coordinate system of the crack B_2. By combining the Equations (4) and (5), the stress tensor expressed in the coordinate system B_2 can be approximated by a polynomial expression with respect to coordinate system B_2. The computation of K_1 requires the coefficients of the polynomial stresses orthogonal to the crack plane (opening mode), i.e. the term in the first row and first column of the stress tensor $\sum^{B_2}$.

As a result, the data are retrieved from the FE model only once per time step, all the crack simulations are performed from the data of the same grid and only linear regression has to be performed for each simulated crack position. As the data transfer between FE software and external post-processing software is time consuming, this strategy allows us to significantly reduce the computational time of the crack simulation procedure.

3.5. Reliability Analysis

The failure probability P_f is the integral of the probability density function on the failure domain. This integral can be estimated using a finite number of evaluations using the Monte-Carlo simulation method (Lemaire 2013; Dunn and Shultis 2012).:

This approximation is valid for a sufficiently large number of simulations N, usually for $N \geq 100/P_f$. In this study, random variables are divided into two categories depending on the numerical efforts associated with the evaluation of the performance function. The random variables affecting the FE model (C, P_c) are associated with considerable numerical efforts because, for each realization, the FE analysis has to be performed for the whole lifetime. The random variables affecting only the crack $(\theta_p, \theta_o, K_{1scc})$ are less demanding to evaluate because they only require post processing without further evaluation of the FE model. Therefore, to allow for large number of simulations and to use the advantage of the variables associated with moderate numerical effort, the Monte-Carlo simulations are carried out on two levels with two different numbers of simulations. This method was first investigated by Weitz and al. (2016) as an improvement of the Monte-Carlo method in such cases. The random variable set can be divided into two sets $\mathbf{X} = (\mathbf{X_1}, \mathbf{X_2})$, where $\mathbf{X_1} = (C, P_c)$ and $\mathbf{X_2} = (\theta_p, \theta_o, K_{1scc})$. Equation can be written as:

$$P_f = \int_{-\infty}^{+\infty} I(\mathbf{x}) f(\mathbf{x}) d\mathbf{x} = \iint_{-\infty}^{+\infty} I(\mathbf{x_1}, \mathbf{x_2}) f_1(\mathbf{x_1}) f_2(\mathbf{x_2}) d\mathbf{x_1} d\mathbf{x_2} \quad (6)$$

where I is the classification function returning 1 in the failure domain and 0 otherwise. The Monte-Carlo simulation is applied twice in order to transform both integrals into sums.

$$P_f \approx \int_{-\infty}^{+\infty} \frac{1}{N_2} \sum_{k=1}^{N_2} I\left(\mathbf{x}_1, \mathbf{x}_2{}^{(k)}\right) d\mathbf{x}_1 \approx \frac{1}{N_1 N_2} \sum_{j=1}^{N_1} \left(\sum_{k=1}^{N_2} I\left(\mathbf{x}_1{}^{(j)}, \mathbf{x}_2{}^{(k)}\right) \right) \quad (7)$$

With this strategy $N_1.N_2$ evaluations of I are available for each time step. They are coming from N_1 evaluations on the FE model and, for each of them, evaluating the stress intensity factor resulting from N_2 simulated cracks. It allows us to choose N_1 and N_2 according to the respective computation time of the FE model and the post-processing, instead of being limited by the most time-consuming. In this study, 500 simulations of the variables related to the finite element model (N_1) are evaluated and 100,000 cracks (N_2) are simulated for each of them and for each time step (t) until complete corrosion of the overpack. Therefore, the failure probability is expressed as follows:

$$P_f(t) \approx \frac{1}{N_1 N_2} \sum_{k=1}^{N_2} \sum_{j=1}^{N_1} I\left(\theta_p{}^{(k)}, \theta_o{}^{(k)}, K_{1scc}{}^{(k)}, C^{(j)}, P_c{}^{(j)}, t\right) \quad (8)$$

where I is associated to the performance function g:

$$g\left(\mathbf{x}_1{}^{(j)}, \mathbf{x}_2{}^{(k)}, t\right) = K_{1scc}{}^{(k)} - K_1\left(\theta_p{}^{(k)}, \theta_o{}^{(k)}, C^{(j)}, P_c{}^{(j)}, t\right) \quad (9)$$

hen full corrosion is reached (i.e. corrosion of all the wall thickness of the overpack), the water can be in contact with the primary package which defines the failure of the system. Therefore, the failure occurs either by propagation of the initial crack or by complete corrosion of the overpack thickness. The corrosion state is checked by comparing the maximal corroded thickness to the initial thickness. The simulation procedure is detailed in the flow chart presented in figure **9**.

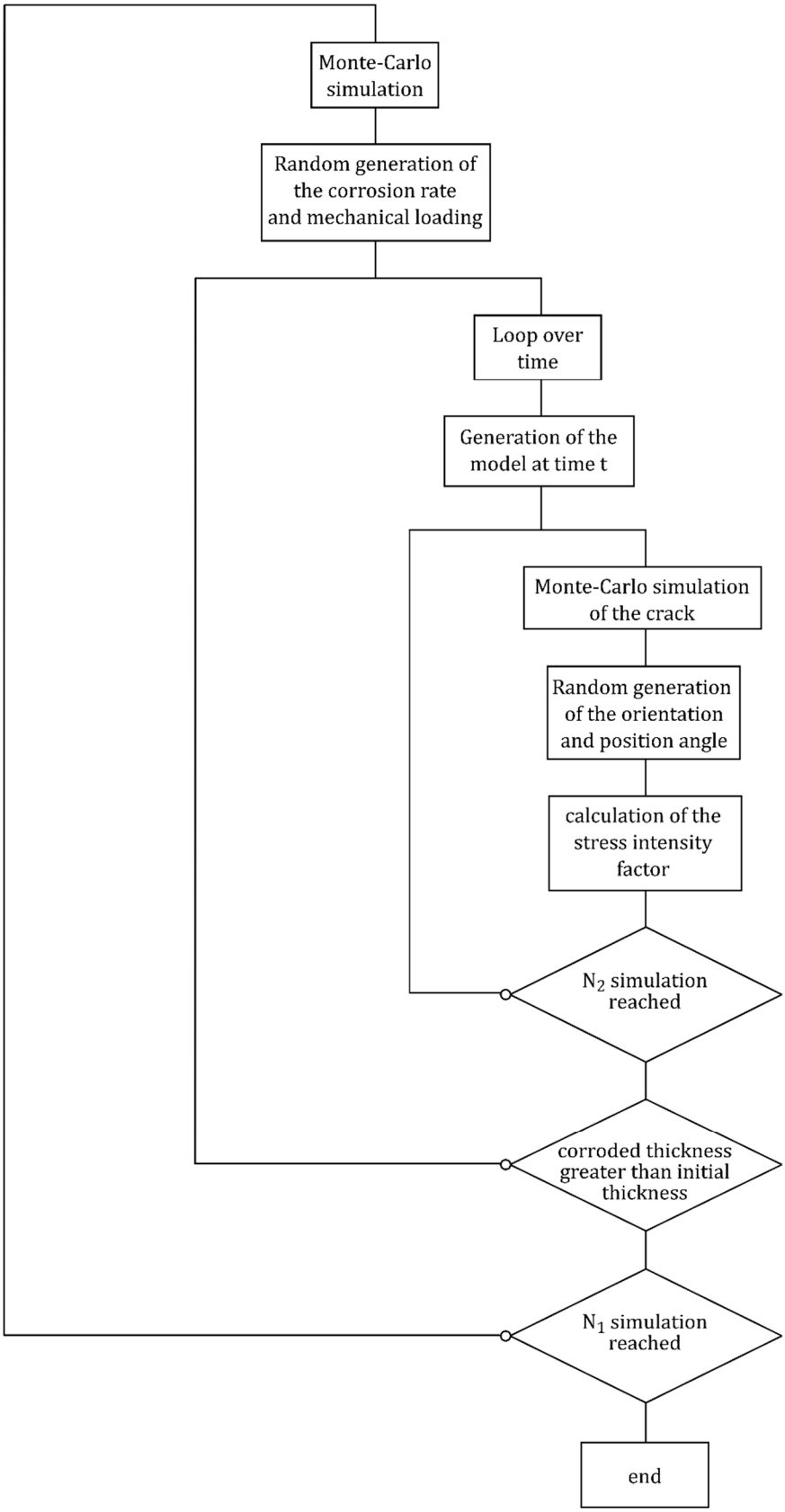

Figure **9.** Flow chart of the simulation procedure

The computing time issue of the Monte-Carlo method has also motivated the development of other

methods known as the advanced Monte-Carlo methods such as Subset simulations (Au and Patelli 2016) and Line Sampling (M. de Angelis, Patelli, and Beer 2015). Unfortunately, these methods are not designed for using on a two-level Monte-Carlo and cannot be directly applied in such cases. The two-level approach has been chosen over the advanced Monte-Carlo methods because of the strong difference in the computational effort of the two levels and the flexibility it offers in the computational time management

3.6. Sensitivity of the result regarding the input parameters

An important outcome of this study is to identify the parameters with large influence on the failure probability. This knowledge allows us to focus engineering efforts on the most important variables to improve the design of the system and more generally to get a better understanding of the studied system. This is the purpose of sensitivity analysis, the applied strategy here consists in identifying the input parameters with large influence on the model output (the value of the stress intensity factor).

The input-output relationship is studied with a scatterplot method (Hamby 1994). The idea is first to perform Monte-Carlo simulations and then to display the output as a function of the value of only one of the inputs. If the output is significantly dependent of the considered input and if enough realisations are available, the scatterplot reveals a relationship pattern and its sharpness gives information about the strength of the relationship. As the problem is time-dependent, the sensitivity analysis can be performed at each time step. The simulations are also performed on two levels implying two different numbers of simulations. The sensitivity analysis is performed separately on each level and in order to free one analysis from the other level, the considered values are:

$$\mathrm{K}_1(\mathbf{x}_1) = \int_{-\infty}^{+\infty} \mathrm{K}_1(\mathbf{x}_1, \mathbf{x}_2) f(\mathbf{x}_2) \mathrm{d}\mathbf{x}_2$$

$$\mathrm{K}_1(\mathbf{x}_2) = \int_{-\infty}^{+\infty} \mathrm{K}_1(\mathbf{x}_1, \mathbf{x}_2) f(\mathbf{x}_1) \mathrm{d}\mathbf{x}_1$$

3.7. Influence of the choice of the distribution on the failure probability

The considered distribution for the random variables are based on expert's opinion which is inaccurate unless when based on several opinions (Ayyub 2001; O'Hagan 2006). Therefore, the real distributions of the parameters may differ from the fitted ones. Hence, the influence of such an event on the validity of the conclusions regarding the reliability of the overpack is investigated. For the sake of this analysis five alternative distributions are considered for the variables associated with high computational effort; i.e. the contact pressure $\mathrm{P_c}$ and the corrosion rate C. Two alternative lognormal distributions are considered with the same mode as the reference distribution, but the interval provided by the expert is now assumed to fit five or seven times the standard deviation. Three additional distributions are tested and chosen to be bounded distribution (triangular, log-triangular and beta distributions) with bounds fitting the confidence interval and the mode equal to the nominal value given by the expert. (The α parameter of the beta distribution is chosen arbitrarily to be equal to two).

The approach of this study is to change the density of the studied random variables and to draw the new evolution curve of the failure probability. The effect is then studied graphically without using dedicated sensibility indicators. The most direct approach would be to conduct Monte-Carlo simulations using the

alternative distributions. However the computational efforts would be significant. Therefore a different approach is used; it is based on a reweighting strategy which may be compared to importance sampling (Rubinstein and Kroese 2008). The main idea is to estimate something about a distribution using observations form a different distribution (Sergienko et al. 2012; Papaioannou, Breitung and Straub 2018; Hesterberg 1996, de Angelis, Patelli, and Beer 2013). As introduced in section 3.5 if the random variable **X** follows an alternative distribution $\bar{f}$, the alternative failure probability is expressed as:

$$P_{\bar{f}} = \int_{-\infty}^{+\infty} I(\mathbf{X}) \bar{f}(\mathbf{X}) d\mathbf{X}$$

Then the numerator and denominator of the expression can be multiplied by the reference density f:

$$P_{\bar{f}} = \int_{-\infty}^{+\infty} I(\mathbf{X}) \frac{f(\mathbf{X})}{f(\mathbf{X})} \bar{f}(\mathbf{X}) d\mathbf{X} = \int_{-\infty}^{+\infty} I(\mathbf{X}) \frac{\bar{f}(\mathbf{X})}{f(\mathbf{X})} f(\mathbf{X}) d\mathbf{X} \quad (10)$$

Then the Monte-Carlo principle can be applied and the integral is turned into a sum of samples $\mathbf{X}_f^{(j)}$ generated following the reference density f:

$$P_{\bar{f}} \approx \frac{1}{N} \sum_{j=1}^{N} I\left(\mathbf{x}_f^{(j)}\right) \frac{\bar{f}\left(\mathbf{x}_f^{(j)}\right)}{f\left(\mathbf{x}_f^{(j)}\right)} \quad (11)$$

This expression denotes that the alternative failure probability can be estimated with weighted realisations of **X** following the reference distribution f. The main benefit of this approach is that the sample of realisations of the random variables following the reference density and their output $I\left(\mathbf{X}_f^{(j)}\right)$ is already available from the Monte-Carlo simulation. Therefore the alternative failure probability can be estimated without further evaluation of the FE model. Comparing the estimated failure probability with the reference one give information about the influence of changes in the distribution of each random variable. The goal is to assess the robustness of the model without performing additional simulations.

4. Results

4.1. Failure probability

The failure probability over time is estimated with the two level Monte Carlo method presented in section 3.5. The FE model is evaluated using 500 realisations of the pressure contact (P_c) and the corrosion rate (C) for time steps of 100 years until complete corrosion of the model. At each time step an independent linear elastic calculation is carried out considering the relevant corroded geometry and mechanical loading. For each evaluation and at each time step the stress intensity factor is estimated for simulated cracks resulting from 100.000 realisations of the position angle (θ_n) and the orientation angle (θ_o). Finally for each evaluation the values of the stress intensity factor (K_1) are compared to 100.000 realisations of the critical stress intensity factor (K_{1scc}).

The simulations are carried out sequentially with Abaqus and the evaluation of one time series (one realisation of P_c and C) takes about 2h on an Intel Core i7-6700 CPU with 32 Go of memory. The 100.000 post-processing calculations associated with the time series take about the same time (2h). The FE calculations and the post-processing can be carried out independently and simultaneously.

In order to increase the accuracy of the estimation for the small probabilities, 500 additional evaluation of the FE model and for each 200.000 crack simulations are performed for 8 time steps between 1000

and 1700 years. This period corresponds to the first failures observed, therefore increasing the size of the evaluated sample allows us to estimate the failure probability more accurately.

The resulting stress intensity factors (K_1) are represented in fig.**10.a** in terms of median value and upper bound of the 95% confidence interval over time. A negative stress intensity factor value is obtained when the equations proposed by Pommier et al. (1999) are applied to a crack subject to a compressive loading. These values are considered equal to zero in the processing of the results which does not affect the median curve nor the estimation of the failure probability (P_f). The curves prove that the dispersion of the stress intensity factor increases with time while the median value increases very slowly. It is observed that cracks are almost equally likely to be subject to a compressive or tensile loading. Therefore, the median value of the stress intensity factor remains close to zero. However, with time increases, the mechanical loading increases and the resulting stress in the material increases as well. As a result, the scatter of the stress intensity factor increases with time (and in turns the upper quantiles of the stress intensity factor are increased). The latest part of the confidence interval curve exhibits irregular shape, this result comes from the decreasing number of realisations available to estimate the values of interest. The reason is that once the FE model is completely corroded it cannot be evaluated anymore. Therefore, with time increasing, more and more realisations among the 500 FE evaluations are lacking in the results of the K_1 values until no value remains available at 3500 years. This constraint causes the 95% confidence interval and the median value to be evaluated with decreasing accuracy along the time, affecting the shape of the curve at late stages.

The figure **10.b** shows the failure probability over time. No failure is observed until 1100 years where the failure probability is 7.3×10^{-8} and P_f is equal to one at 3500 years. The failure probability at 500 years (i.e. the specified lifetime of the overpack) is lower than 7.3×10^{-8} no failure occurred at this time.

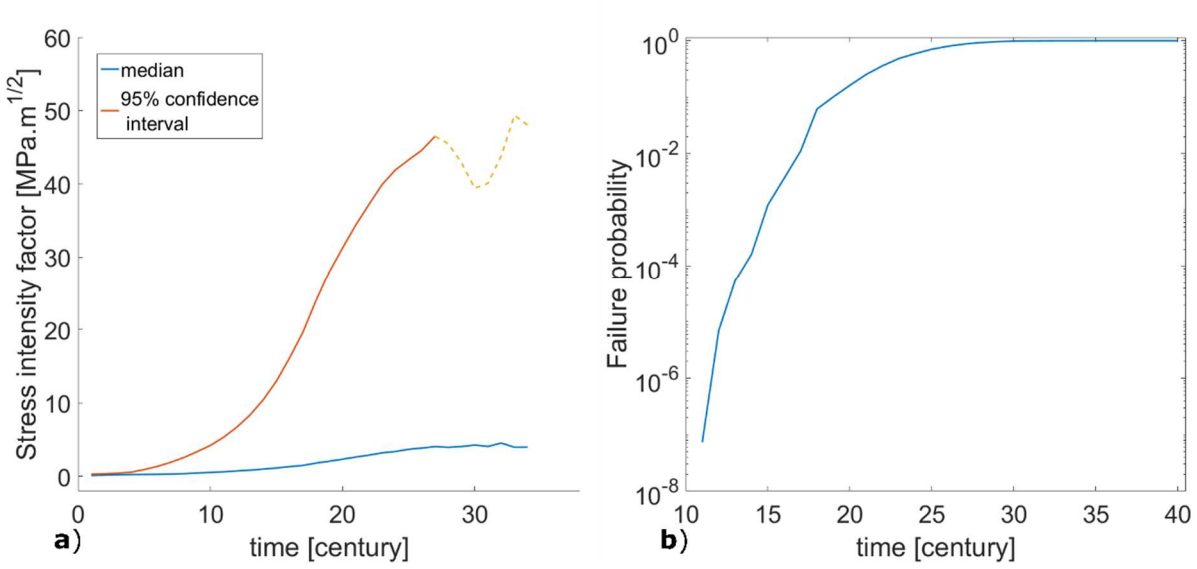

Figure **10.a.** Median value and upperbound of the 95% confidence interval of the K_1 values over time. **b.** Estimated failure probability over time in semi logarithmic scale.

4.2. Parameter sensitivities

The sensitivity analysis is conducted with scatterplot analysis as detailed in section 3.6. The values are studied for two time steps arbitrarily selected at 200 and 1700 years to investigate the correlations at both early and late stages of the lifetime, and the results are presented respectively in figures 10 and 11. The presented values of the stress intensity factor are averaged with respect to the level of simulations $\mathbf{x}_2$ for figures **11** and **12** (**a.** and **b.**) and the level $\mathbf{x}_1$ for figures **11** and **12** (**c.** and **d.**) as introduced in

section 3.6.

At 200 years, a sharp and direct dependence is visible between the mean value of the stress intensity factor (K_{1mean}) and the corrosion rate (fig. **11.a**), proving that the corrosion rate has a strong influence on the model response. On the contrary, the mean value of the stress intensity factor has a weak dependence on the contact pressure at early stages (fig. **11.b**) (i.e. increasing or decreasing the contact pressure seems not to have any influence on the stress intensity factor variation). This result is linked to the buckling time of the liner, which is uncertain because it depends on the corrosion rate, but at early stages it is very likely that the buckling of the liner has not yet occurred. Therefore, the contact pressure has a very weak influence on the output because in most of the simulations, the overpack is only subjected to an external fluid pressure and all the variability may be associated with the uncertainties of the corrosion rate.

The pattern exhibited by the scatterplot of the position angle θ_p (fig. **11.c**) is as well distinctive of variables having no correlation at all. For the orientation angle θ_o a really sharp dependence is visible again (fig. **11.d**), the correlation is not linear, it is more likely to be periodic, considering the nature of the involved random variable. It proves that the orientation angle has a strong influence on the mean stress intensity factor at the early stages of the lifetime. This result is linked as well to the buckling of the liner. Before buckling, the mechanical loading is only a uniform external pressure. Therefore, the stress field does not depend on the circumferential position, and neither does the mean stress intensity

factor. As a result, the variations depend only on the orientation of the crack.

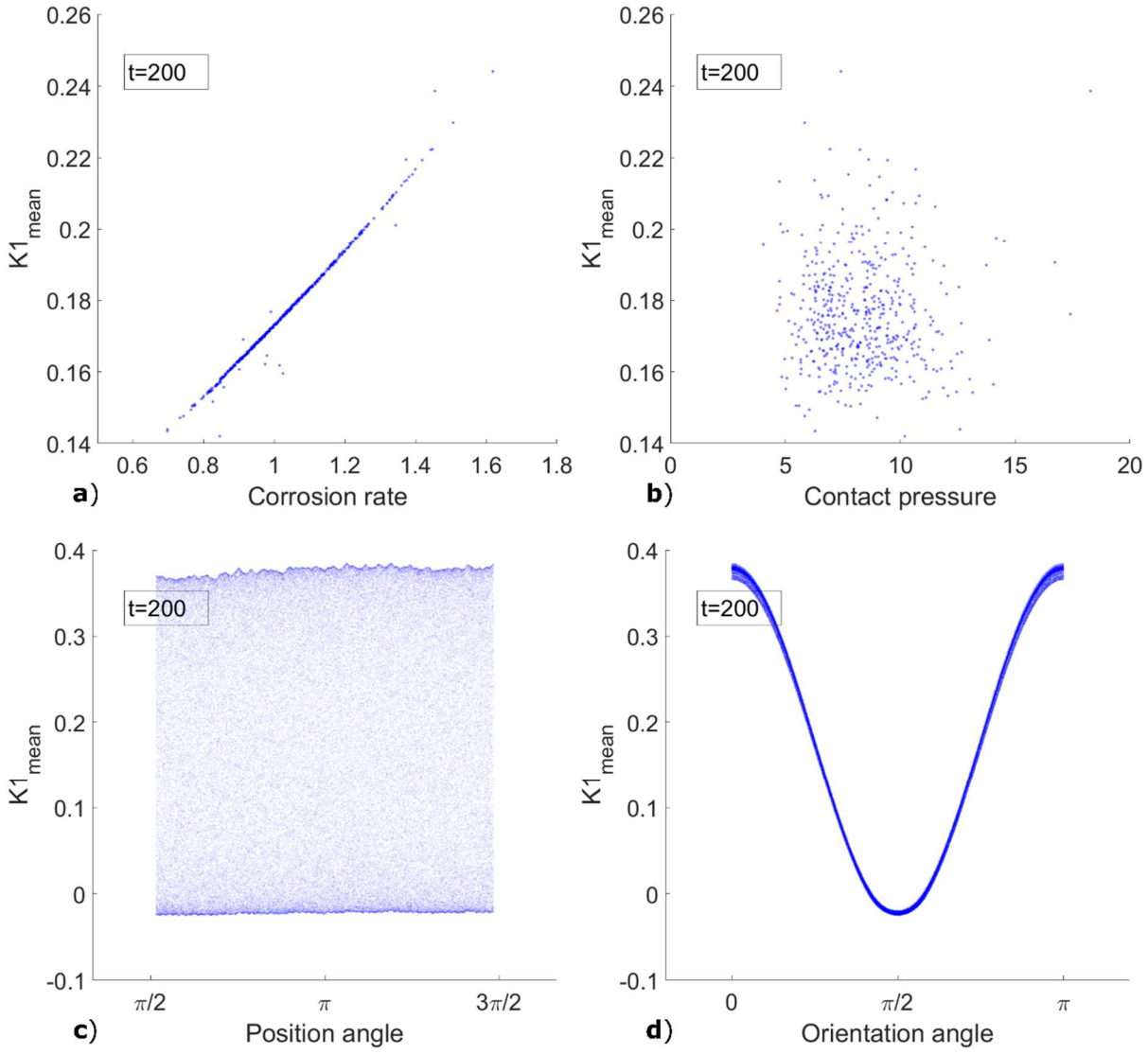

Figure **11.** Scatterplot of the mean stress intensity factor $[MPa\sqrt{m}]$ at 200 years with respect to: **a.** the corrosion rate; **b.** the contact pressure $[MPa]$; **c.** the position angle; **d.** the orientation angle.

At 1700 years, the conclusions about the corrosion rate and the contact pressure are mainly the same as before: the corrosion rate has a stonger influence on the mean stress intensity factor than the contact pressure even though it is observed that the contact pressure has a slight influence (fig.**12.a, b**). This result proves that even after the liner buckling, the corrosion rate is more critical than the contact pressure.

Regarding the position and orientation angles of the crack, the conclusions drawn at 200 years are no longer valid. A strong relationship can be observed between the position angle and the mean stress intensity factor; and the relationship with respect to the orientation angle is weaker and seems multi-modal (fig. **12.c, d**). The result can be explained mainly by the non-uniform mechanical loading. Once the buckling of the liner occured, the stress field in the material depends strongly on the circumferential position. Therefore, the position of the crack has a significant influence on the model response. In the mean time, the orientation of the crak still implies a variation of the average stress intensity factor, but the interval in wich these variations are contained is driven by the crack position. After a while, the variations due to the position angle become significantly bigger than the variations due to the orientation

angle and the influence of the latter paremeter decreases. It can also be noted that the asymetry in the pattern of the scatterplot of the position angle is due to the non uniform thickness of the overpack induced by the corrosion process.

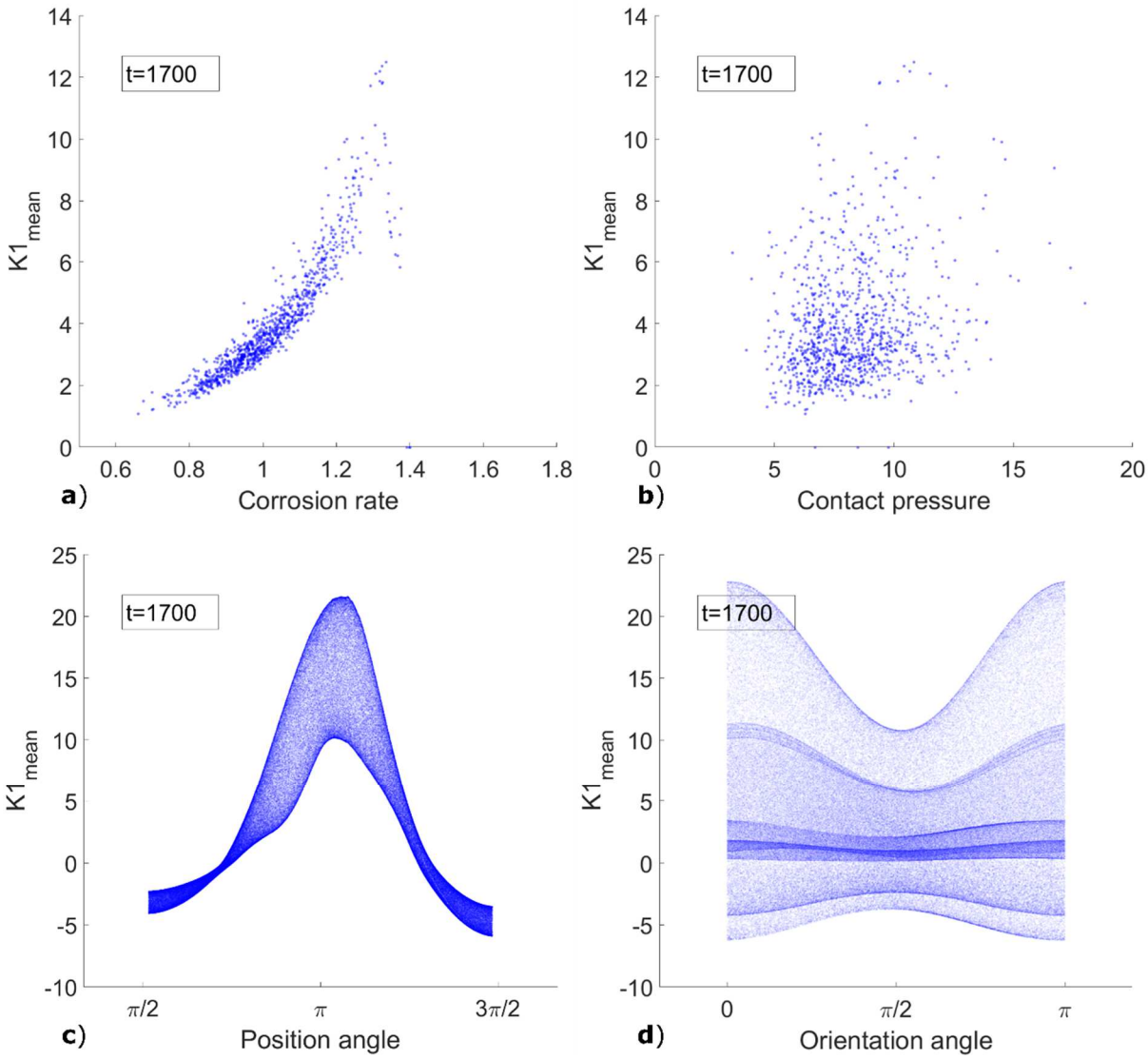

Figure **12.** Scatterplot of the mean stress intensity factor $[MPa\sqrt{m}]$ at 1700 years with respect to: **a.** the corrosion rate; **b.** the contact pressure $[MPa]$; **c.** the position angle; d. the orientation angle.

4.3. Impact of the choice of the distributions

The impact of the choice of the distributions is studied herein by changing the distributions of both of random variables obtained using expert judgement: the corrosion rate and the contact pressure. The failure probability curves resulting from different choices of standard deviation of the corrosion rate and the contact pressure are presented in figure **13.a**. As detailed in section 3.7 two alternative distributions considering that the amplitude of the credible interval is five and seven times the standard deviation are studied. They are respectively referred to as the 2.5σ and 3.5σ distributions and are compared to the reference 3σ distribution. The standard deviation of the 2.5σ distribution is greater than the reference one, therefore the resulting failure probability is also greater. For the same reason, the 3.5σ distribution induces a smaller failure probability. The re-weighting method employed is less precise when the

standard deviation of the simulated distribution is greater than the reference distribution. That is the reason why the failure probability curve for the 2.5σ distribution is less smooth than the reference one.

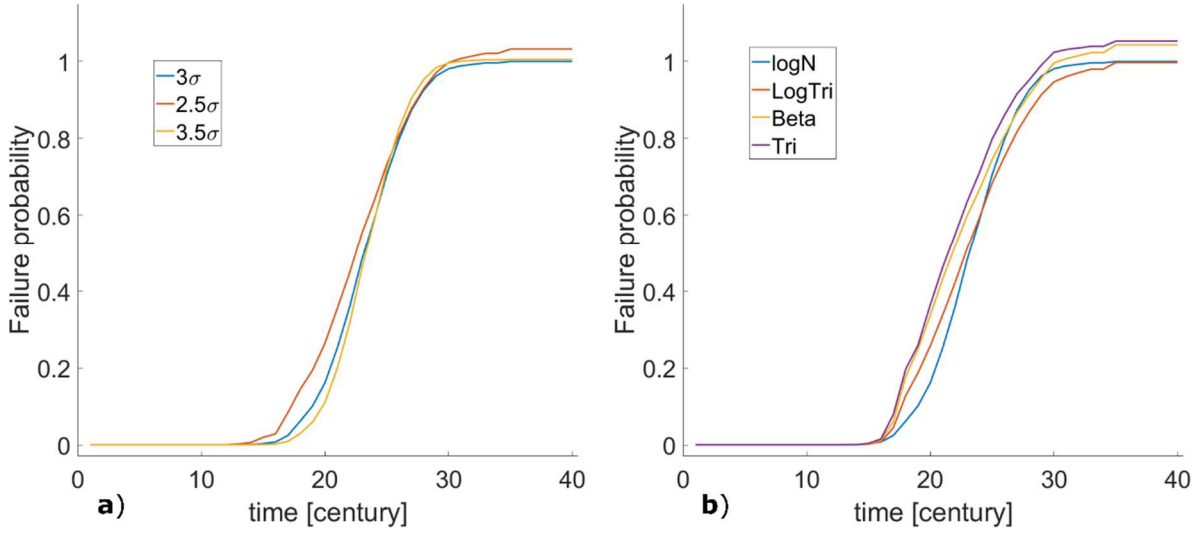

Figure **13.** Failure probability considering alternative distributions for the corrosion rate and the contact pressure: **a.** the 2.5, 3 and 3.5σ lognormal distributions; **b.** the reference lognormal distribution, a log-triangular, a beta and a triangular distribution.

The failure probability resulting from the corrosion rate and the contact pressure following triangular, log-triangular and beta distributions are presented in figure **13.b**. The distribution that shifts the curve the most is the triangular distribution, and all of the tested distributions lead to an increase of the early failure probability. However, the effect is sufficiently limited to not contradict the conclusions about the reliability of the system at 500 years. All the simulated failure probability curves exhibit a long-term stabilised value close to 1, the observed scatter is due to the re-weighting method and the limited amount of available data.

5. Conclusions

A methodology is presented for the evaluation of the failure probability of HLW overpacks. A stochastic and time-dependent structural model is developed. The finite element model takes into account the corrosion process, the mechanical loading, the presence of a surface crack and the uncertainties in the fracture mechanics properties of the material. The uncertainties related to these phenomena are studied using five random variables for which the distributions are elicitated from expert's judgement.

A reliability analysis is performed with a two-level Monte Carlo method in order to reduce the numerical efforts. From these numerical investigations it was found that the failure probability of the system at 500 years is small enough to ensure the system safety target. The first observed failures are at 1100 years inducing a very low failure probability.

Sensitivity analyses are conducted to check the first order impact of the input parameters on the uncertainties of the structure response. It is observed that the corrosion rate is the most critical parameter. Therefore, this phenomenon needs to be further studied in case where more accurate estimation of the failure probability becomes necessary.

Many distributions can result from expert's opinions elicitation, several different distributions are tested and the influence of them on the failure probability is observed. This analysis is conducted using a re-

weighting method to avoid further evaluations of the model. The results do not contradict the conclusions about the reliability of the system at 500 years.

Further studies are still ongoing, among them, different life scenarios of the overpack are considered plausible and should be tested, depending for example on different resaturation/desaturation kinetics of the disposal cell. Moreover, different failure scenarios corresponding to the ductile fracture of the overpack will be tested. This failure mode, which will however result in a lower failure probability than brittle fracture, is indeed more likely to occur due to the very low sensitivity to SCC of non-alloy steels in repository condition.

6. Acknowledgement

This work is founded by Andra, which is gratefully acknowledged for the technical and financial support. The authors would like to gratefully thank Didier Crusset, Valerie Deydier and Sophia Necib for the helpful discussions on corrosion modes expected in repository conditions.

7. References

AFNOR. 1998. 'Non-Destructive Testing of Steel Forgings. Ultrasonic Testing of Ferritic or Martensitic Steel Forgings'. NF EN 10228-3.

Alexander W. R., and McKinley L. 2007. *Deep Geological Disposal of Radioactive Waste*. 1st ed. Vol. Volume 9. Radioactivity in the Environmen. Elsevier Science.

Amirat, A., A. Mohamed-Chateauneuf, and K. Chaoui. 2006. 'Reliability Assessment of Underground Pipelines under the Combined Effect of Active Corrosion and Residual Stress'. *International Journal of Pressure Vessels and Piping* 83 (2): 107–17. https://doi.org/10.1016/j.ijpvp.2005.11.004.

ANDRA. 2005. 'Dossier 2005 Synthesis Argile: Tome Phenomenological Evolution of a Geological Repository'.

Angelis, Marco de, Edoardo Patelli, and Michael Beer. 2015. 'Advanced Line Sampling for Efficient Robust Reliability Analysis'. *Structural Safety* 52 (January): 170–82. https://doi.org/10.1016/j.strusafe.2014.10.002.

Angelis, M De, E Patelli, and M Beer. n.d. 'An Efficient Strategy for Computing Interval Expectations of Risk', In Safety, Reliability, Risk and Life-Cycle Performance of Structures & Infrastructures. ICOSSAR 2013, June 16-20, 2013, Ch299, 2225--2232."

Au, Siu-Kui, and Edoardo Patelli. 2016. 'Rare Event Simulation in Finite-Infinite Dimensional Space'. *Reliability Engineering & System Safety* 148 (April): 67–77. https://doi.org/10.1016/j.ress.2015.11.012.

Ayyub, B. M. 2001. *Elicitation of Expert Opinions for Uncertainty and Risks*. Boca Raton, Fla: CRC Press.

Bhargava, Kapilesh, Yasuhiro Mori, and A.K. Ghosh. 2011. 'Time-Dependent Reliability of Corrosion-Affected RC Beams—Part 1: Estimation of Time-Dependent Strengths and Associated Variability'. *Nuclear Engineering and Design* 241 (5): 1371–84. https://doi.org/10.1016/j.nucengdes.2011.01.005.

Broggi, M., and G.I. Schuëller. 2011. 'Efficient Modeling of Imperfections for Buckling Analysis of Composite Cylindrical Shells'. *Engineering Structures* 33 (5): 1796–1806. https://doi.org/10.1016/j.engstruct.2011.02.019.

Bumbieler, F., S. Nécib, J. Morel, D. Cruset, and G. Armand. 2015. 'Mechanical and SCC Behavior of an API5L Steel Casing Within the Context of Deep Geological Repositories for Radioactive Waste'. *ASME 2015 Pressure Vessels and Piping Conference*, 19 July 2015.

Chijimatsu, M., T.S. Nguyen, L. Jing, J. De Jonge, M. Kohlmeier, A. Millard, A. Rejeb, J. Rutqvist, M. Souley, and Y. Sugita. 2005. 'Numerical Study of the THM Effects on the Near-Field Safety of a Hypothetical Nuclear Waste Repository—BMT1 of the DECOVALEX III Project. Part 1: Conceptualization and Characterization of the Problems and Summary of Results'.

International Journal of Rock Mechanics and Mining Sciences 42 (5–6): 720–30. https://doi.org/10.1016/j.ijrmms.2005.03.010.
Croisé, J., G. Mayer, J. Talandier, and J. Wendling. 2011. 'Impact of Water Consumption and Saturation-Dependent Corrosion Rate on Hydrogen Generation and Migration from an Intermediate-Level Radioactive Waste Repository'. *Transport in Porous Media* 90 (1): 59–75. https://doi.org/10.1007/s11242-011-9803-0.
Dundulis, G., I. Žutautaitė, R. Janulionis, E. Ušpuras, S. Rimkevičius, and M. Eid. 2016. 'Integrated Failure Probability Estimation Based on Structural Integrity Analysis and Failure Data: Natural Gas Pipeline Case'. *Reliability Engineering & System Safety* 156 (December): 195–202. https://doi.org/10.1016/j.ress.2016.08.003.
Dunn, W L., and J K. Shultis. 2012. *Exploring Monte Carlo Methods*. Amsterdam ; Boston: Elsevier/Academic Press.
Goller, B., M. Broggi, A. Calvi, and G.I. Schuëller. 2011. 'A Stochastic Model Updating Technique for Complex Aerospace Structures'. *Finite Elements in Analysis and Design* 47 (7): 739–52. https://doi.org/10.1016/j.finel.2011.02.005.
Hamby, D. M. 1994. 'A Review of Techniques for Parameter Sensitivity Analysis of Environmental Models'. *Environmental Monitoring and Assessment* 32 (2): 135–54. https://doi.org/10.1007/BF00547132.
Hari Prasad, M., G. Rami Reddy, P.N. Dubey, A. Srividya, and A.K. Verma. 2013. 'Reliability Estimation of Structures under Stochastic Loading—A Case Study on Nuclear Piping'. *Nuclear Engineering and Design* 254 (January): 185–93. https://doi.org/10.1016/j.nucengdes.2012.09.017.
Hesterberg, T.C. 1996. 'Estimates and Confidence Intervals for Importance Sampling Sensitivity Analysis'. *Mathematical and Computer Modelling* 23 (8–9): 79–85. https://doi.org/10.1016/0895-7177(96)00041-6.
Hoorelbeke, J.M. 2009. 'Conteneurs pour le stockage des déchets HA et MAVL', 19.
International Atomic Energy Agency. 2001. 'The Use of Scientific and Technical Results from Underground Research Laboratory Investigations for the Geological Disposal of Radioactive Waste'.
International Energy Agency. 2017. 'Electricity Information 2017', 683.
Kim, S H., M S. Choi, J Y. Joung, and K S. Kim. 2013. 'Long-Term Reliability Evaluation of Nuclear Containments with Tendon Force Degradation'. *Nuclear Engineering and Design* 265 (December): 582–90. https://doi.org/10.1016/j.nucengdes.2013.06.025.
Lemaire, M. 2013. *Structural Reliability*. John Wiley & Sons.
Levy, S. 2010. 'Need for USA High Level Waste (HLW) Alternate Geological Repository (AGR) and for a Different Methodology to Enhance Its Acceptance'. *Nuclear Engineering and Design* 240 (10): 3665–68. https://doi.org/10.1016/j.nucengdes.2010.06.036.
Lidskog, R., and A.-C. Andersson. 2002. 'The Management of Radioactive Waste. A Description of Ten Countries.' http://www.skb.se/publication/19408/The%20management.pdf.
Necib, S., F. Bumbieler, C. Duret-Thual, N. Bulidon, D. Crusset, and P. Combrade. 2017. 'Assessment of the Resistance to Environmentally Assisted Cracking (EAC) of C-Steel Casing and Overpack in the CO *x* Claystone'. *Corrosion Engineering, Science and Technology* 52 (sup1): 95–100. https://doi.org/10.1080/1478422X.2017.1336003.
Newman, J. C., and I. S. Raju. 1981. 'An Empirical Stress-Intensity Factor Equation for the Surface Crack'. *Engineering Fracture Mechanics* 15 (1–2): 185–192.
Nguyen, T. 2017. 'Flambage Sous Contact d'une Coque Cylindrique Soumise à Pression Externe'. Lyon: INSA.
O'Hagan, A., ed. 2006. *Uncertain Judgements: Eliciting Experts' Probabilities*. Statistics in Practice. London ; Hoboken, NJ: John Wiley & Sons.
Papaioannou, L., K. Breitung, and D. Straub. 2018. 'Reliability Sensitivity Estimation with Sequential Importance Sampling'. *Structural Safety* 75 (November): 24–34. https://doi.org/10.1016/j.strusafe.2018.05.003.
Patelli, E., H. Murat Panayirci, M. Broggi, B. Goller, P. Beaurepaire, H J. Pradlwarter, and G I. Schuëller. 2012. 'General Purpose Software for Efficient Uncertainty Management of Large

Finite Element Models'. *Finite Elements in Analysis and Design* 51 (April): 31–48. https://doi.org/10.1016/j.finel.2011.11.003.
Pommier, S, C Sakae, and Y Murakami. 1999. 'An Empirical Stress Intensity Factor Set of Equations for a Semi-Elliptical Crack in a Semi-Infinite Body Subjected to a Polynomial Stress Distribution.' *International Journal of Fatigue* 21 (3): 243–51. https://doi.org/10.1016/S0142-1123(98)00074-7.
Rempe, Norbert T. 2007. 'Permanent Underground Repositories for Radioactive Waste'. *Progress in Nuclear Energy* 49 (5): 365–74. https://doi.org/10.1016/j.pnucene.2007.04.002.
Rubinstein, Reuven Y., and Dirk P. Kroese. 2008. *Simulation and the Monte Carlo Method*. 2nd ed. Wiley Series in Probability and Statistics. Hoboken, N.J: John Wiley & Sons.
Schlegel, M.L., C. Bataillon, F. Brucker, C. Blanc, D. Prêt, E. Foy, and M. Chorro. 2014. 'Corrosion of Metal Iron in Contact with Anoxic Clay at 90 °C: Characterization of the Corrosion Products after Two Years of Interaction'. *Applied Geochemistry* 51 (December): 1–14. https://doi.org/10.1016/j.apgeochem.2014.09.002.
Schuëller, G.I. 1989. 'Reliability of Nuclear Structures'. *Nuclear Engineering and Design* 114 (2): 235–45. https://doi.org/10.1016/0029-5493(89)90194-5.
Sergienko, E., P. Lemaître, A. Arnaud, D. Busby, and F. Gamboa. 2012. 'Reliability Sensitivity Analysis Based on Probability Distribution Perturbation with Application to CO2 Storage', 16.
Stefanou, G. 2009. 'The Stochastic Finite Element Method: Past, Present and Future'. *Computer Methods in Applied Mechanics and Engineering* 198 (9–12): 1031–51. https://doi.org/10.1016/j.cma.2008.11.007.
Sudret, B., and A. Der Kiureghian. 2002. 'Comparison of Finite Element Reliability Methods'. *Probabilistic Engineering Mechanics* 17 (4): 337–48. https://doi.org/10.1016/S0266-8920(02)00031-0.
Valdebenito, M.A., and G.I. Schuëller. 2010. 'Design of Maintenance Schedules for Fatigue-Prone Metallic Components Using Reliability-Based Optimization'. *Computer Methods in Applied Mechanics and Engineering* 199 (33–36): 2305–18. https://doi.org/10.1016/j.cma.2010.03.028.
Weitz, S., S. Blanco, J. Charon, J. Dauchet, M. El Hafi, Vincent Eymet, Olivier Farges, Richard Fournier, and Jacques Gautrais. 2016. 'Monte Carlo Efficiency Improvement by Multiple Sampling of Conditioned Integration Variables'. *Journal of Computational Physics* 326 (December): 30–34. https://doi.org/10.1016/j.jcp.2016.08.036.